JACS
JOURNAL OF THE AMERICAN CHEMICAL SOCIETY

ARTICLE

pubs.acs.org/JACS

Nanostructured $Ti_{0.7}Mo_{0.3}O_2$ Support Enhances Electron Transfer to Pt: High-Performance Catalyst for Oxygen Reduction Reaction

Van Thi Thanh Ho,[†] Chun-Jern Pan,[†] John Rick,[†] Wei-Nien Su,[†] and Bing-Joe Hwang*[,†,‡,§]

[†]NanoElectrochemistry Laboratory, Department of Chemical Engineering, National Taiwan University of Science and Technology, Taipei 106, Taiwan

[‡]National Synchrotron Radiation Research Center, Hsinchu 30076, Taiwan

Supporting Information

ABSTRACT: The slow rate of the oxygen reduction reaction (ORR) and the instability of Pt-based catalysts are two of the most important issues that must be solved in order to make proton exchange membrane fuel cells (PEMFCs) a reality. Additionally, the serious carbon corrosion on the cathode side is a critical problem with respect to the durability of catalyst that limits its wide application. Here, we present a new approach by exploring robust noncarbon $Ti_{0.7}Mo_{0.3}O_2$ used as a novel functionalized cocatalytic support for Pt. This approach is based on the novel nanostructure $Ti_{0.7}Mo_{0.3}O_2$ support with "electronic transfer mechanism" from $Ti_{0.7}Mo_{0.3}O_2$ to Pt that can modify the surface electronic structure of Pt, owing to a shift in the d-band center of the surface Pt atoms. Furthermore, another benefit of $Ti_{0.7}Mo_{0.3}O_2$ is the extremely high stability of $Pt/Ti_{0.7}Mo_{0.3}O_2$ during potential cycling, which is attributable to the strong metal/support interaction (SMSI) between Pt and $Ti_{0.7}Mo_{0.3}O_2$. This also enhances the inherent structural and chemical stability and the corrosion resistance of the TiO_2-based oxide in acidic and oxidative environments. We also demonstrate that the ORR current densities generated using cocatalytic $Pt/Ti_{0.7}Mo_{0.3}O_2$ are respectively ~7- and 2.6-fold higher than those of commercial Pt/C and PtCo/C catalysts with the same Pt loading. This new approach opens a reliable path to the discovery advanced concept in designing new catalysts that can replace the traditional catalytic structure and motivate further research in the field.

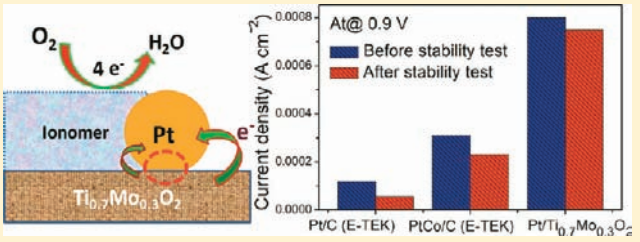

1. INTRODUCTION

Fuel cell technology is believed to have the potential to become a major source of clean energy[1,2] with particularly important applications in transportation. Despite considerable recent advances, existing fuel-cell technology still needs to be improved,[3−5] especially with respect to the pivotal role of the oxygen reduction reaction (ORR) in proton exchange membrane fuel cells (PEMFCs), where the extremely corrosive conditions of the fuel-cell cathode require that the catalyst be chemically active enough to activate O_2 and yet noble enough to release the oxygen in the form of H_2O. The slow rate of the oxygen reduction reaction and instability of Pt on the cathode side are the main factors limiting its wide application.[1−8] Numerous investigations have been carried out to improve the activity and durability of Pt for ORR. For instance, a series of binary Pt−M alloys with late transition metals (M = Cr, Mn, Co, Ni)[9] and early transition metals (M = Sc, Y)[10] or dealloying of some alloys of Pt,[11,12] as well as synthesis of platinum core−shell catalyst,[13] are routes to make Pt-based catalysts more active than pure Pt catalysts. The enhancement of activity and durability of these binary Pt−M alloys is based on electronic transfer mechanisms of the second transition metal (M) to Pt, which modified the surface electronic structure of Pt, owing to a shift in the d-band center of the surface Pt atoms that results in a weakened interaction between Pt and intermediate oxide species, freeing more active sites for O_2 adsorption.[9−13] However, one of the difficulties in making these systems form surface Pt overlayers or "skins", by using thermal treatments at high temperature or acid treatments such as is the case of PtCo or PtNi catalysts, is also a limitation for commercialization of this technology.[14] Additionally, studies indicate that under acidic conditions the Pt−M alloys may exhibit instability and lose oxygen reduction activity due to leaching/dissolution of the transition metals, leading to a reduction in to the long-term durability of the catalysts.[14−16]

Yet catalyst stability in PEMFCs is also a critical hurdle and key challenge to their commercialization in stationary and transportation power applications.[17−19] Currently, fuel-cell technology uses carbon black[20,21] as a catalyst support for both the anodes and cathodes. However, the predominance of weak interactions between the carbon support and the catalytic metal nanoparticles leads to sintering of the catalytic metal nanoparticles and a consequent decrease in the active surface area with long-term operation.[22−25] More important, the high potentials that accelerate both electrochemical carbon corrosion and dissolution of the active elements under normal operating conditions are issues

Received: April 29, 2011
Published: June 27, 2011

impacting fuel-cell durability that remain unresolved.[26−29] To solve these issues, several recent studies have concentrated on developing materials that exhibit corrosion resistance, including some with a higher graphitic character, such as: nanofibers,[30] carbon nanotubes,[31] carbon nanocages,[32] and graphene.[33] These nanostructured carbons show a severalfold lower intrinsic corrosion rate; however, they do not prevent carbon oxidation.[29] Recently, much attention has been centered on the development of robust non-carbon support materials, such as highly stable conducting metal oxides, that can prevent the carbon corrosion[27,28] or introduce a synergistic cocatalytic effect between Pt and the conducting metal oxide support such as highly CO-tolerant electrocatalytic activity for hydrogen oxidation.[34]

Here, we present a new approach by exploring a robust novel non-carbon-based cocatalytic support material comprising $Ti_{0.7}Mo_{0.3}O_2$ to support the Pt nanoparticles (NPs). Interestingly, this approach can solve the above issues due to the various advantages conferred by the multifunctional $Ti_{0.7}Mo_{0.3}O_2$. These advantages are in terms of its high surface area, porosity, and the strong Pt interactions that lead to highly dispersed and well-anchored Pt catalyst particles. More specifically, the $Ti_{0.7}Mo_{0.3}O_2$ support acts as a cocatalyst, supporting Pt activity, based on "electronic transfer mechanisms" from $Ti_{0.7}Mo_{0.3}O_2$ to Pt; that is, the shift in the d-band structure of the Pt NPs leads to weak interactions between Pt and the intermediate species, which is normally played by the second metal in the conventional Pt−M system, thereby, promoting the reduction of oxygen in a manner that a simple carbon support cannot. Additionally, the combination of ultrahighly stable TiO_2[35,36] with MoO_x[37] noted for its high electronic conductivity and relative stability in acid solutions, is used as an new approach to develop a multifunctional support material for Pt that exhibits much improved activity and durability over commercial Pt/C and PtCo/C catalysts for oxygen reduction reaction for potential application in PEMFCs.

2. EXPERIMENTAL SECTION

2.1. Synthesis of $Ti_{0.7}Mo_{0.3}O_2$ Nanoparticles. $Ti_{0.7}Mo_{0.3}O_2$ NPs were synthesized by a single-step hydrothermal process, at low temperature as a low-energy-consuming fabrication technique[38] that did not employ a surfactant or stabilizer. An aqueous solution containing 12 mM $MoCl_5$ and 28 mM $TiCl_4$ precursors (with Mo:Ti = 3:7 molar ratio) was prepared. The precursor solution was then transferred to a Teflon-lined autoclave with a stainless steel shell and heated to 200 at 10 °C·min^{-1} in an oven. The sample was kept at 200 °C for 2 h in the oven and then cooled to room temperature. $Ti_{0.7}Mo_{0.3}O_2$ was washed with water and collected by centrifugation several times until the washings showed pH 7. The precipitates were dried at 80 °C in a vacuum oven overnight (>8 h) for the electrochemical and textural analyses.

2.2. Synthesis of Pt/$Ti_{0.7}Mo_{0.3}O_2$ Catalyst. Platinum NPs were anchored over the $Ti_{0.7}Mo_{0.3}O_2$ support by a microwave-assisted polyol synthesis. The synthesis was carried out with the aid of a domestic microwave oven (LG MG-5021MW1, 300 W, 2450 MHz). Platinum (intake 20 wt %) was deposited as follows: 2.0 mL of 50 mM hexachloroplatinic acid in ethylene glycol was added to 30 mL of ethylene glycol to produce a yellowish solution. $Ti_{0.7}Mo_{0.3}O_2$ (80 mg) was mixed with the solution containing hexachloroplatinic acid and the mixture was ultrasonicated for 30 min, followed by the addition of sodium hydroxide (0.8 M) to adjust the pH to 11.0. The suspension was exposed in the middle of a microwave oven for 1 h at 200 W (160 °C). When the reaction was complete, the sample was cooled in air and the black precipitate was collected by repeated centrifugation and washed with acetone and deionized water. The resulting Pt/$Ti_{0.7}Mo_{0.3}O_2$ was dried at 80 °C in a vacuum oven overnight. For comparison, the same amount of Pt was deposited on undoped TiO_2 (20 wt % Pt/undoped TiO_2) and MoO_2 (20 wt % Pt/MoO_2) following the same procedure.

2.3. Material Characterization. Powder X-ray diffraction (XRD) patterns of $Ti_{0.7}Mo_{0.3}O_2$ and Pt/$Ti_{0.7}Mo_{0.3}O_2$ nanocatalysts were obtained with XRD-Rigaku Dmax-B, Japan measurements using Cu Kα radiation and Ni as filter at 40 kV and 100 mA. The data were collected from 20° to 90° in 2θ scale with a scan rate of 2°·min^{-1}. The particle sizes of $Ti_{0.7}Mo_{0.3}O_2$ and Pt/$Ti_{0.7}Mo_{0.3}O_2$ NPs were evaluated by transmission electron microscopy (TEM) on an FEI-TEM-2000 microscope operated at an accelerating voltage of 3800 V. Specimens were prepared by ultrasonically suspending the NPs in ethanol; the suspension was then applied to a copper grid and dried in an oven.

The Pt loading on support was determined both by energy-dispersive X-ray spectroscopy (EDX-JSM 6500F, JEOL) with an accelerating voltage of 15 kV and by inductively coupled plasma atomic emission spectrometry (ICP-AES). Average composition of the $Ti_{0.7}Mo_{0.3}O_2$ support and elemental mapping of the Pt/$Ti_{0.7}Mo_{0.3}O_2$ catalyst were also obtained by use of an EDX-JSM 6500F, JEOL, with an accelerating voltage of 10 kV. The Brunauer−Emmett−Teller (BET) surface area and pore size of the $Ti_{0.7}Mo_{0.3}O_2$ support were obtained from N_2 adsorption isotherms at 77 K (Porous Materials, BET-202A). Before the BET measurement, the material was degassed/dried at 250 °C for 3 h in order to completely vaporize the water molecules adsorbed in the meso/micropores of the oxide. Accordingly, the BET data shown here correspond to the annealed samples. The electrical conductivity of the $Ti_{0.7}Mo_{0.3}O_2$ powder was measured by a standard four-probe technique (KeithLink Technology, Taiwan). $Ti_{0.7}Mo_{0.3}O_2$ powder was made into pellets, of ∼13 mm diameter and ∼1 mm thickness, by use of a steel die in a hydraulic press under a pressure of 300 MPa. To obtain reliable electrical conductivity data, the four-point probe system was carefully placed on the $Ti_{0.7}Mo_{0.3}O_2$ pellet, at three different sites on each sample. For comparison, the electronic conductivity of the undoped TiO_2 was measured under the same conditions as the $Ti_{0.7}Mo_{0.3}O_2$ powder measurement.

X-ray absorption spectra (XAS) were recorded at the National Synchrotron Radiation Research Centre (NSRRC) of Taiwan, beamline 01 C, following the procedure described in detail elsewhere.[39,40] Experimental details, such as instrument specifications, cell configuration, and sample treatment for proper measurement, were the same as before. Measurements were made at room temperature with solid samples. Mo foil, MoO_2, and MoO_3 were used as references for Mo K-edge measurements, as was a Pt foil for Pt L_{III}-edge measurements and Ti foil for the Ti $L_{2,3}$-edge. The control of parameters for extended X-ray absorption fine structure (EXAFS) measurements, data collection modes, and calculation of errors were all done as per the guidelines set by the International XAFS Society Standards and Criteria Committee.[39,40]

2.4. Electrode Preparation and Electrochemical Measurements. A three-electrode cell connected to a Solartron 1480 potentiostat/galvanostat was used for electrochemical measurements. A high surface area Pt and a saturated calomel electrode were used as counter-electrode and reference electrode, respectively. All potentials in this work are referred to a normal hydrogen electrode (NHE). A thin layer of Nafion-impregnated Pt/$Ti_{0.7}Mo_{0.3}O_2$ catalyst cast on a glassy carbon disk (PINE) of 5 mm diameter (0.1964 cm^2 area) embedded in a Teflon holder was the working electrode. A known amount of Pt/$Ti_{0.7}Mo_{0.3}O_2$ catalyst was dispersed in 0.5% Nafion by sonication for 3 h, and 7 μL of catalyst suspension containing 6.2 mg of Pt·mL^{-1} was placed on the glassy carbon electrode (GCE) surface and dried at 80 °C for 15 min to yield a uniform thin film of the catalyst. Prior to catalyst coating, GCE surface was cleaned by polishing with 0.3 μm alumina powder (BAS), cleaned with ethanol, and washed with copious amounts of deionized water. An aqueous solution of H_2SO_4 (0.5 M) was used as the electrolyte in all the electrochemical measurements. In cyclic voltammetry (CV),

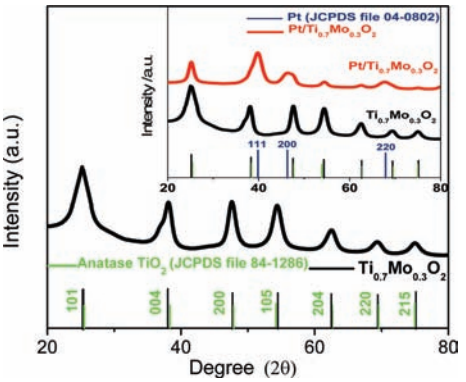

Figure 1. X-ray diffraction patterns of $Ti_{0.7}Mo_{0.3}O_2$ support material and (inset) $Pt/Ti_{0.7}Mo_{0.3}O_2$ catalyst.

potential was swept between 0.05 and 1.10 V at a scan rate (ν) of 25 mV·s^{-1}. Prior to the CV measurements, the electrode was activated in the same solution by potential cycling 10 times in the range 0.05−1.10 V at ν = 50 mV·s^{-1}. Steady-state polarization measurements of ORR were carried out from 0 to 1.1 V at ν = 1 mV·s^{-1} with the electrode being rotated at 1600 rpm. Electrode stability tests were performed by continuous potential cycling (CV) up to 5000 cycles in the potential window 0−1.10 V at ν = 50 mV·s^{-1}, and steady-state polarization in ORR was measured after 5000 cycles in the range from 0 to 1.1 V at ν = 1 mV·s^{-1} with the electrode being rotated at 1600 rpm. To undertake electrochemical measurements, working electrodes comprising Nafion-impregnated commercial catalysts [Pt/C (E-TEK) or PtCo/C (E-TEK)] on GCE were prepared following the same procedure as above. Pt loading was maintained at 0.221 mg·cm^{-2} on all the catalyst electrodes in the electrochemical studies. In addition to the ORR performance measurements, the $Pt/Ti_{0.7}Mo_{0.3}O_2$ and commercial Pt/C and PtCo/C catalysts were evaluated via a linear sweep in oxygen-saturated 0.1 M $HClO_4$ at 25 °C at a rotation rate of 1600 rpm and at ν = 10 mV·s^{-1} within a potential range from 0 to 1.1 V versus NHE.

3. RESULTS AND DISCUSSION

3.1. Characterization of $Ti_{0.7}Mo_{0.3}O_2$ Support Material. The structure of the $Ti_{0.7}Mo_{0.3}O_2$ samples was confirmed by X-ray diffraction (XRD) measurements. Figure 1 shows the diffraction peaks of $Ti_{0.7}Mo_{0.3}O_2$ at 2θ positions 25.1°, 38.1°, 47.5°, 54.4°, and 62.5° that can be indexed to a unit cell, shifted slightly from that of pure anatase-TiO_2 (JCPDS file 84-1286) due to the molybdenum doping. No signal corresponding to a single metallic phase of Mo or to phase separation between molybdenum and titanium oxide (Figure 1), was detected, confirming that $Ti_{0.7}Mo_{0.3}O_2$ is principally a single-phase solid solution with anatase phase of TiO_2 structure. This finding is supported by the transmission electron microscopy (TEM) image of $Ti_{0.7}Mo_{0.3}O_2$ (Figure 2), showing a solid solution comprised of fine nanoparticles 8−10 nm. The very good crystallinity of $Ti_{0.7}Mo_{0.3}O_2$ (Figure 2, inset) is also clearly apparent from the well-defined fringes at ∼3.4 Å that correspond to the spacing of the {101} plane of anatase TiO_2: this is in good accord with the XRD pattern. Energy-dispersive X-ray spectroscopic (EDX) measurements (Figure S1, Supporting Information), indicated a Ti:Mo atomic ratio of 69.32:30.68, which agrees closely with the expected atomic ratio of 70:30 for $Ti_{0.7}Mo_{0.3}O_2$. This suggests that the composition of the (Ti:Mo) binary metal oxide can be controlled in a facile manner by adjusting the ratios of $MoCl_5$ and $TiCl_4$ in the precursor

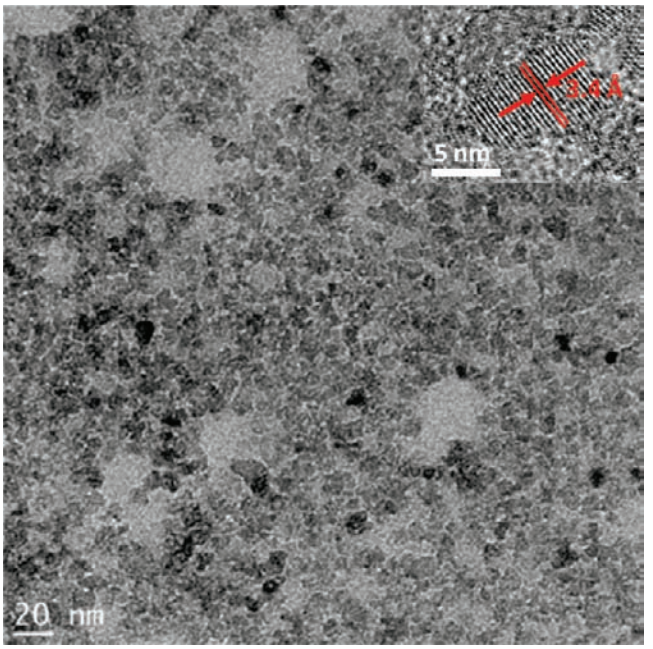

Figure 2. TEM image of $Ti_{0.7}Mo_{0.3}O_2$ support material and (inset) HRTEM of $Ti_{0.7}Mo_{0.3}O_2$.

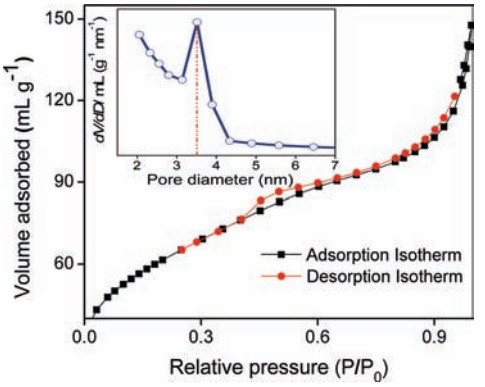

Figure 3. Nitrogen adsorption/desorption isotherms of $Ti_{0.7}Mo_{0.3}O_2$ support and (inset) its corresponding Barrett−Joyner−Halenda (BJH) pore size distribution.

solutions without the need for any template or reductant. The nitrogen sorption (adsorption and desorption) isotherm and its corresponding Barrett−Joyner−Halenda (BJH) pore size distribution for the new $Ti_{0.7}Mo_{0.3}O_2$ support material are shown in Figure 3. The $Ti_{0.7}Mo_{0.3}O_2$ support exhibits a typical type IV isotherm with a distinct hysteretic loop, attributable to the presence of mesopores in $Ti_{0.7}Mo_{0.3}O_2$; this deduction is supported by the pore size distribution curve (Figure 3, inset) showing the pore size center at ∼3.5 nm for $Ti_{0.7}Mo_{0.3}O_2$. In addition, the BET measurements showed that $Ti_{0.7}Mo_{0.3}O_2$ possesses a high surface area (230 m^2·g^{-1})—a critical requirement for catalyst support material—comparable to the well-known Vulcan XC72 (232 m^2·g^{-1}).[41] The electronic conductivity of the $Ti_{0.7}Mo_{0.3}O_2$ nanoparticles was measured as approximately 2.8×10^{-4} S·cm^{-1}, which is significant higher than that of the undoped TiO_2 nanoparticles (1.37×10^{-7} S·cm^{-1}).

In order to better understand the oxidation state of Mo in the $Ti_{0.7}Mo_{0.3}O_2$ structure, the molybdenum valence was determined

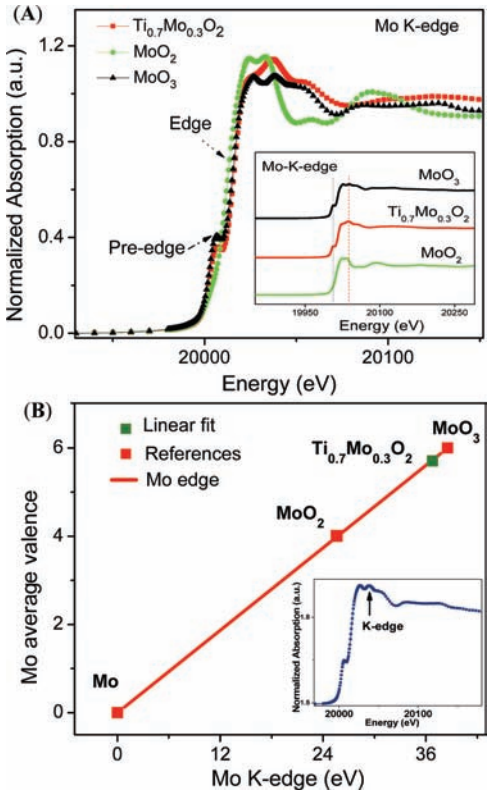

Figure 4. (A) Mo K near-edge spectra of $Ti_{0.7}Mo_{0.3}O_2$ and molybdenum oxides used as references (MoO_2, MoO_3). (B) Molybdenum average valence of $Ti_{0.7}Mo_{0.3}O_2$ and Mo oxide references in panel A as a function of the Mo K-edge position and (inset) the inserted feature used to determine the K-edge position.

from the Mo K-edge X-ray absorption near-edge structure (XANES) (Figure 4A). The shift of the Mo K-absorption edge to higher phonon energies with respect to the metal standard gives information about the valence of Mo, while the pre-edge features correspond to its coordination geometry.[42] The XANES spectrum of standard MoO_3 shows a strong pre-edge peak that arises from an allowed 1s−4d electronic transition for tetrahedral symmetry.[43] This characteristic can also be observed as a shoulder for $Ti_{0.7}Mo_{0.3}O_2$. However, in the spectrum of standard MoO_2, where Mo is in a regular octahedron, this feature is not observed. Additionally, the oxidation state of Mo can be derived from the energy shift of the X-ray absorption edge[44] (Figure 4B). The linear fit of the Mo average valence, obtained by use of a feature above the edge position (K-edge, inset), has been determined as a best fit to the data[45] from three references sample (Mo, MoO_2, and MoO_3 references). Figure 4B shows the calculated average Mo valence state in $Ti_{0.7}Mo_{0.3}O_2$ to be 5.75, which is representative of the molybdenum oxide's mixed oxidation state.

3.2. Characterization of Pt/$Ti_{0.7}Mo_{0.3}O_2$ Catalyst. The formation of crystalline Pt nanoparticles in Pt/$Ti_{0.7}Mo_{0.3}O_2$ catalyst was verified by XRD patterns (inset, Figure 1). Pt/$Ti_{0.7}Mo_{0.3}O_2$ gave four characteristic diffraction peaks corresponding to (111), (200), (220), and (311) of the face-centered cubic (fcc) Pt (JCPDS file 04-0802), in addition to the strong reflections corresponding to the $Ti_{0.7}Mo_{0.3}O_2$ support. This finding is further is confirmed by TEM. It can be observed that the small, uniformly distributed, darkly contrasting spherical Pt nanoparticles (3−4 nm diameter)

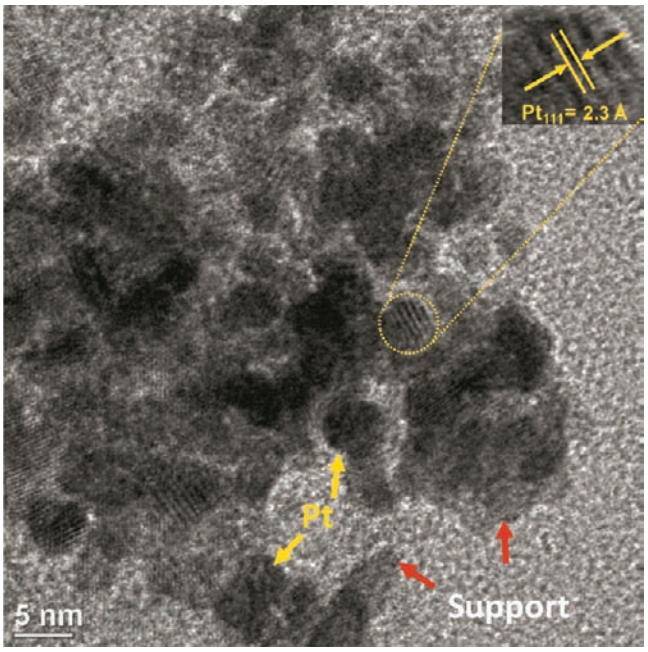

Figure 5. TEM image of Pt/$Ti_{0.7}Mo_{0.3}O_2$ catalyst.

are well adhered to the $Ti_{0.7}Mo_{0.3}O_2$ support (Figure 5 and Figure S2, Supporting Information) though no pretreatment (e.g., heat treatment, acid treatment, or polymer wrapping) steps were used. The fringes with lattice spacings of 2.3 Å can be indexed as {111} of fcc Pt as shown in Figure 5, indicating the existence of good crystallinity of Pt NPs anchored on the $Ti_{0.7}Mo_{0.3}O_2$ support. Pt loading on the $Ti_{0.7}Mo_{0.3}O_2$ support was determined by both inductively coupled plasma atomic emission spectrometry (ICP-AES) analysis (18.15 wt % Pt) and EDX (18.36 wt % Pt) (Figure S3, Supporting Information). These values agreed very well with the calculated 20 wt % used in the catalyst's preparation. The uniform distributions of elements in a Pt/$Ti_{0.7}Mo_{0.3}O_2$ catalyst were verified through elemental mapping using SEM-EDX (Figure S4, Supporting Information) as well as via TEM imaging (Figure 5). Interestingly, there was no signal of metallic Mo or valence state change of molybdenum oxide even after Pt deposition (Figure S5, Supporting Information), which corresponds to the XRD data. These results confirm that $Ti_{0.7}Mo_{0.3}O_2$ is highly stable and robust with a large surface area, enabling the Pt NPs to be well distributed on the support.

In order to gain insight into the geometric structure and identify the electronic properties of the oxidation states of Pt/$Ti_{0.7}Mo_{0.3}O_2$, X-ray absorption spectroscopy was used. The XANES region of Pt/$Ti_{0.7}Mo_{0.3}O_2$ has been plotted and compared to commercial 20 wt % Pt/C (E-TEK) and 30 wt % PtCo(1:1)/C (E-TEK) catalysts(see Figure 6A). It is interesting to note that the intensity of the white line, whose magnitude is a direct measure of d-band vacancies, is in the order Pt/C (E-TEK) ≥ Pt foil > PtCo/C (E-TEK) > Pt/$Ti_{0.7}Mo_{0.3}O_2$,with Pt/$Ti_{0.7}Mo_{0.3}O_2$ showing the lowest intensity. The changes in the white-line intensity in principle could be caused by size effects and/or electronic effects.[40,46,47] Note that the particle sizes of Pt/$Ti_{0.7}Mo_{0.3}O_2$, Pt/C (E-TEK), and PtCo/C (E-TEK) were similar (data not shown here); thus, the particle sizes being of similar dimensions, the changes in the white-line intensity for these catalyst samples are primarily a manifestation of electronic

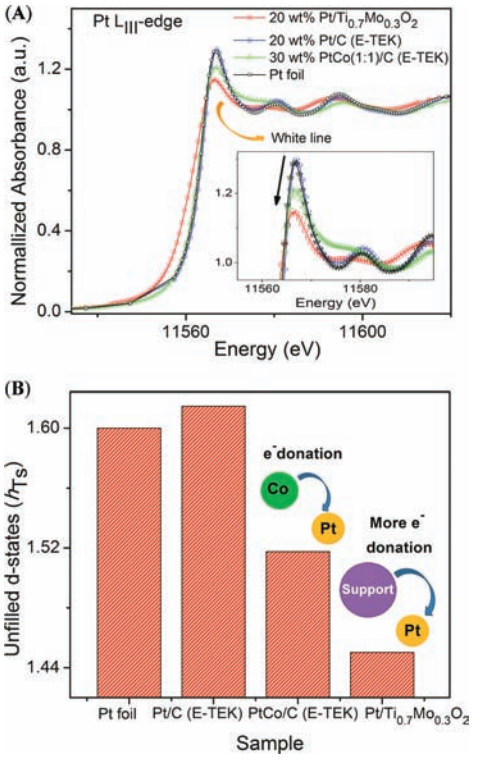

Figure 6. (A) Pt L_{III}-edge XANES spectra and (B) variation in unfilled d-states for Pt foil and different catalyst samples (denoted in the figure). (Inset) Enlarged region of peaks of Pt L_{III}-edge XANES white line.

effects that induce changes in the d-band vacancy of Pt. In a similar manner, the intensity decrease for PtCo/C (E-TEK) compared to Pt/C (E-TEK) can be easily understood as being due to electron transfer from Co to Pt, leading to a high electron density around the Pt atoms and hence a decrease in the Pt d-band vacancy.[48] Interestingly, in the case of Pt/$Ti_{0.7}Mo_{0.3}O_2$ with only one catalyst component (Pt), the large decrease in its white-line intensity arises from a different origin; namely, the strong metal/support interaction (SMSI)[49−51] between Pt and the $Ti_{0.7}Mo_{0.3}O_2$ support. This mechanism explains the facile nature of electron donation from the $Ti_{0.7}Mo_{0.3}O_2$ support to Pt metal, leading ultimately to a drastic decrease in the d-band vacancy of Pt, as reflected in the results of the calculation to determine the number of unfilled d states (h_{Ts}) (see details in Supporting Information).[39,40] The Pt/$Ti_{0.7}Mo_{0.3}O_2$ catalyst shows the lowest number of unfilled d-states (h_{Ts} = 1.45) compared to all the other samples, viz., PtCo/C (h_{Ts} = 1.55), Pt/C catalyst (h_{Ts} = 1.62), and Pt foil (h_{Ts} = 1.60) in Figure 6B. Additional evidence for the synergistic effect in Pt/$Ti_{0.7}Mo_{0.3}O_2$ NPs was obtained from the Ti $L_{2,3}$-edge (2p → 3d) of the XAS spectra between $Ti_{0.7}Mo_{0.3}O_2$ and Pt/$Ti_{0.7}Mo_{0.3}O_2$ (Figure 7). It can be seen that the Ti $L_{2,3}$-edge XAS spectra for $Ti_{0.7}Mo_{0.3}O_2$ and Pt/$Ti_{0.7}Mo_{0.3}O_2$ are consistent with that of anatase-TiO_2,[52] seen in the XRD pattern. The main features of the spectrum are caused by the dipole transition from the 2p core to 3d unoccupied states.[53] It is worth noting that the intensity of Pt/$Ti_{0.7}Mo_{0.3}O_2$ increases for all features compared to $Ti_{0.7}Mo_{0.3}O_2$ (inset in Figure 7). This increase directly reflects an increase in the number of Ti vacancies, leading to an increase in the number of Ti 3d holes because of electron donation from the $Ti_{0.7}Mo_{0.3}O_2$ support to Pt: this is in very good correspondence

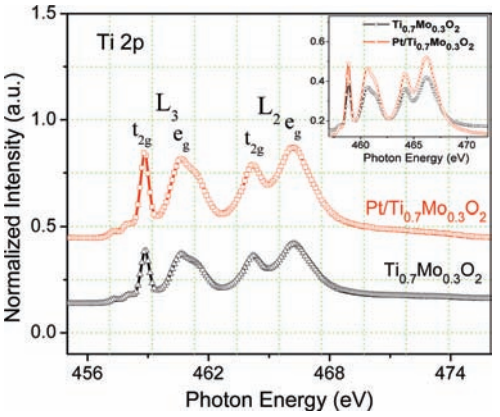

Figure 7. XAS spectra of Ti $L_{2,3}$-edge of $Ti_{0.7}Mo_{0.3}O_2$ and Pt/$Ti_{0.7}Mo_{0.3}O_2$ samples. (Inset) XAS spectra of Ti $L_{2,3}$-edges with different intensity in Pt/$Ti_{0.7}Mo_{0.3}O_2$ and $Ti_{0.7}Mo_{0.3}O_2$ samples.

with the Pt L_{III}-edge as discussed previously (Figure 6). These results indicate clearly that the SMSI between $Ti_{0.7}Mo_{0.3}O_2$ and Pt, which results in facile electron donation from the $Ti_{0.7}Mo_{0.3}O_2$ support to Pt metal, leads ultimately to a drastic decrease in the d-band vacancy of Pt. Therefore, $Ti_{0.7}Mo_{0.3}O_2$ can play an important role as cocatalyst for noble Pt metal, which is normally played by the second metal in the conventional Pt−M system that a simple carbon support cannot.

Furthermore, the local structure of Pt atoms in the Pt/$Ti_{0.7}Mo_{0.3}O_2$ and commercial Pt/C and PtCo/C catalysts was investigated by extended X-ray absorption fine structure (EXAFS) with a reference Pt foil. The corresponding Fourier transforms (FT) of k^2-weighted EXAFS oscillations at the Pt L_{III}-edge are shown in Figure 8A. The peak centered at 2.5 Å represents the contribution of the first metal−metal coordination shell to the EXAFS oscillations. The similarity of the FT features indicates that the Pt phase, present in the Pt/$Ti_{0.7}Mo_{0.3}O_2$ catalyst, is similar to that in Pt/C (E-TEK) and corresponds to Pt foil having the fcc structure of bulk platinum. It is apparent that the magnitude of this peak for Pt/$Ti_{0.7}Mo_{0.3}O_2$ and the commercial catalysts Pt/C and PtCo/C is smaller for these dispersed catalysts compared to that of bulk Pt, due to the very small particle size. The peak splitting in the case of bimetallic nanoparticles in PtCo/C catalyst indicates the presence of two types of backscattering atoms in the first shell coordination. Figure 8B depicts the k^2-weighted Pt L_{III}-edge EXAFS spectra collected for Pt/$Ti_{0.7}Mo_{0.3}O_2$ catalyst nanoparticles with various commercial Pt/C and PtCo/C catalysts and a reference Pt foil: excellent data quality, with a high signal-to-noise ratio, was obtained from Pt/$Ti_{0.7}Mo_{0.3}O_2$ catalyst due to the presence of EXAFS oscillations, observed up to 14 $Å^{-1}$.

3.3. Electrochemical Properties of Pt/$Ti_{0.7}Mo_{0.3}O_2$ Catalyst. The catalytic properties of Pt/$Ti_{0.7}Mo_{0.3}O_2$, used as a cathodic material for the ORR in PEMFCs, were studied with commercial 20 wt % Pt/C (E-TEK) and 30 wt % PtCo (1:1)/C (E-TEK) catalysts used for comparison. Figure 9 shows cyclic voltammetry (CV) curves of these three catalysts, recorded at room temperature in N_2-purged 0.5 M H_2SO_4 solutions, at a scan rate of 25 $mV \cdot s^{-1}$. The electrochemically active surface area (ECSA) was calculated by measuring the charge collected in the H_{upd} adsorption/desorption region after double-layer correction with a value of 210 $mC \cdot cm^{-2}$ assumed for the adsorption of a hydrogen monolayer.[54] The specific ECSA of the 20 wt %

$Pt/Ti_{0.7}Mo_{0.3}O_2$ (72.5 $m^2 \cdot g^{-1}$) was found to be similar to the Pt/C catalyst (73.7 $m^2 \cdot g^{-1}$) and higher than that of PtCo/C (61.9 $m^2 \cdot g^{-1}$). The highly active surface area of $Pt/Ti_{0.7}Mo_{0.3}O_2$ is attributed to the small size and good dispersion of the Pt catalyst on the porous $Ti_{0.7}Mo_{0.3}O_2$ support that creates a large Pt surface, thereby resulting in a large electrochemically active surface area. Noticeably, no oxidation or reduction peaks appear for molybdenum oxide from the $Pt/Ti_{0.7}Mo_{0.3}O_2$ voltammetric result, suggesting that the molybdenum is introduced into the lattice of anatase TiO_2, which is highly stable in acidic solutions and oxidative environments.[37] Interestingly, the $Ti_{0.7}Mo_{0.3}O_2$-supported Pt, but not the carbon support Pt or PtCo, shows a high double layer capacitance region (see Figure 9); this may be attributed to the capacitive properties of molybdenum oxide[55−57] in the support material that can be created by differences in the structure of the electrodes.

Figure 10 shows the polarization curves of 20 wt % $Pt/Ti_{0.7}Mo_{0.3}O_2$ catalysts compared to commercial 20 wt % Pt/C (E-TEK) and 30 wt % PtCo (1:1)/C (E-TEK) catalysts. As expected, the $Pt/Ti_{0.7}Mo_{0.3}O_2$ catalysts show excellent catalytic activity toward the ORR compared to conventional carbon-supported Pt or PtCo catalyst electrodes. For instance, $Pt/Ti_{0.7}Mo_{0.3}O_2$ has a more positive onset potential (~130 mV) than Pt/C (E-TEK) and an even more positive activity (~80 mV) than PtCo/C (E-TEK), and thus it was more active than the commercial catalysts. The current density, taken from the ORR activity, at the half-wave potential (~0.9 V) is respectively, a 7- and a 2.6-fold improvement over those of the commercial Pt/C and PtCo/C catalysts. Similarly, the $Pt/Ti_{0.7}Mo_{0.3}O_2$ catalyst exhibited a high mass activity at 0.85 V, compared to commercial Pt/C (E-TEK) and PtCo/C (E-TEK) catalysts (Figure S6, Supporting Information). Furthermore, the ORR activity of $Pt/Ti_{0.7}Mo_{0.3}O_2$ catalyst as measured in O_2-saturated

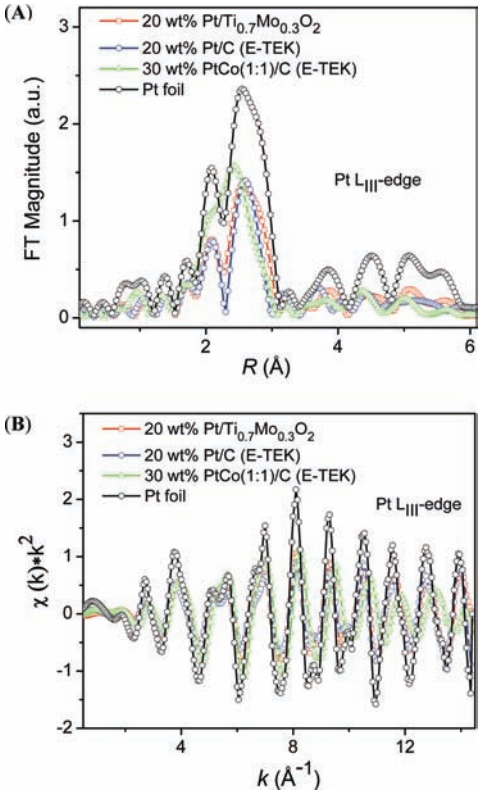

Figure 8. (A) Fourier transforms (FT) of k^2-weighted extended X-ray absorption fine structure (EXAFS) oscillations at the Pt L_{III}-edge and (B) k^2-weighted EXAFS oscillations at the Pt L_{III}-edge spectra collected for $Pt/Ti_{0.7}Mo_{0.3}O_2$ catalyst nanoparticles with various commercial catalysts and reference Pt foil.

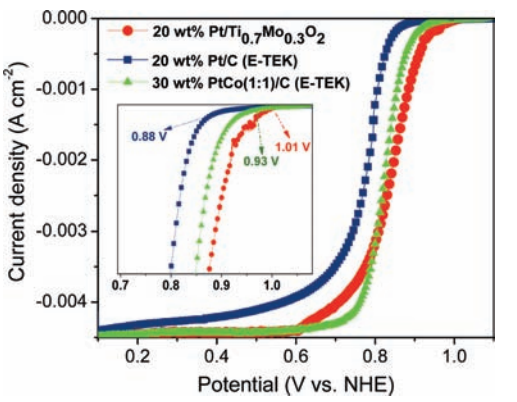

Figure 10. Polarization curves showing the ORR current of $Pt/Ti_{0.7}Mo_{0.3}O_2$ catalyst and two kinds of commercial Pt/C (E-TEK) and PtCo/C (E-TEK) catalysts. The current was normalized to the geometric area of the electrode (0.1964 cm^2), and the electrode rotation rate was kept at 1600 rpm, with a sweep rate of 1 $mV \cdot s^{-1}$ in 0.5 M H_2SO_4 at 25 °C.

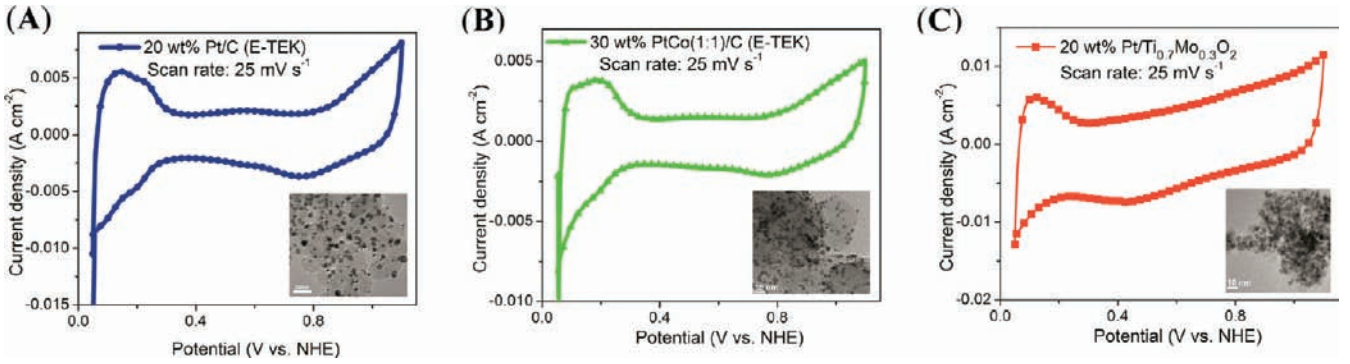

Figure 9. Cyclic voltammograms for (A) 20 wt % Pt/C (E-TEK), (B) 30 wt % PtCo(1:1)/C (E-TEK), and (C) 20 wt % $Pt/Ti_{0.7}Mo_{0.3}O_2$ in N_2-saturated 0.5 M H_2SO_4 solution at 25 °C. Sweep rate = 25 $mV \cdot s^{-1}$; Pt loading of electrodes = 0.221 $mg \cdot cm^{-2}$. (Insets) TEM of $Pt/Ti_{0.7}Mo_{0.3}O_2$ and commercial Pt/C and PtCo/C catalysts (scale bar 10 nm).

dx.doi.org/10.1021/ja2039562 |J. Am. Chem. Soc. 2011, 133, 11716–11724

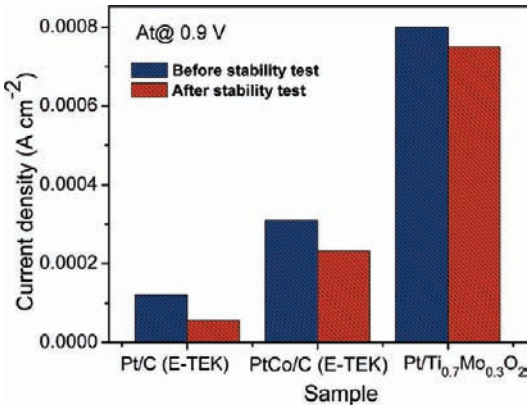

Figure 11. Stability characterization of $Pt/Ti_{0.7}Mo_{0.3}O_2$ and commercial Pt/C (E-TEK) and PtCo/C (E-TEK) catalysts at 0.9 V before and after stability by 5000 potential cycles. The electrode rotation rate was kept at 1600 rpm, with a sweep rate of 1 $mV \cdot s^{-1}$ in 0.5 M H_2SO_4 at 25 °C.

0.1 M $HClO_4$ solutions also shows a significant enhancement of activity with respect to the state-of-the-art Pt/C and PtCo/C catalysts under the same conditions, confirming that the $Pt/Ti_{0.7}Mo_{0.3}O_2$ catalyst is a good electrocatalyst with superior ORR activity (Figure S7, Supporting Information). Thus, the $Pt/Ti_{0.7}Mo_{0.3}O_2$ catalyst outperformed commercial catalysts in catalyzing the ORR, which can be attributed to the advantages conferred by the $Ti_{0.7}Mo_{0.3}O_2$ support over conventional carbon black supports, such as the electronic structure change of Pt when undergoing synergistic interactions with the $Ti_{0.7}Mo_{0.3}O_2$ support. The electron-rich nature of the Pt studied here originates not from the interactions of, for example, Pt-based alloy catalysts or from alloy films (such as Pt—M alloys with M = Fe, Co, Ni),[58] FePt NPs,[59] or Pt_3Ni (111),[60] but was the result of the facile electron transfer from the novel support to the catalytic Pt, leading to a shift in the d-band center of the surface Pt atoms. It is worth noting that this is the main role played by the second metal (M) in conventional Pt—M catalysts systems, while here this role is played well by the $Ti_{0.7}Mo_{0.3}O_2$ support. The bimetal oxide, besides being a robust support material for Pt, also participates strongly in bonding, inducing d-orbital bond strain, leading to a reduced intermediate adsorptive strength for Pt in the rate-determining step (RDS). Thus, more active sites for O_2 adsorption are available that can facilitate a faster catalytic electrode reaction.[51]

The activity of the catalysts in Figure 10 before and after the stability test is depicted in Figure 11. The stability of the catalysts was assessed by applying potential steps between 0.0 and 1.10 V (NHE) in O_2-saturated H_2SO_4 (0.5 M) electrolytes at 25 °C. The $Pt/Ti_{0.7}Mo_{0.3}O_2$ catalyst was also more stable under ORR conditions than the commercial catalysts. Notably, the $Pt/Ti_{0.7}Mo_{0.3}O_2$ catalyst showed no significant diminution in activity after 5000 cycles and only ~8% performance degradation at 0.9 V. In sharp contrast, a serious loss of activity was observed in the corresponding commercial Pt/C (E-TEK) and PtCo/C (E-TEK) catalysts. The activity of Pt/C showed activity degradation of ~50.6%, while PtCo/C was reduced by ~25.8%, suggesting that carbon corrosion at high potentials was responsible for this effect. The much-enhanced ORR stability of the $Pt/Ti_{0.7}Mo_{0.3}O_2$ catalyst may also arise from strong metal/support interactions (SMSI)[49−51] between the Pt particles and the $Ti_{0.7}Mo_{0.3}O_2$ support with tightly bound Pt particles that prevent Pt migration. The good evidence for strong stability from electrochemical tests is consistent with previous predictions from the XANES results.

To gain further understanding of the enhanced efficiency ORR of the nanostructured $Ti_{0.7}Mo_{0.3}O_2$ support, the ORR measurement was performed for 20 wt % Pt/undoped TiO_2, 20 wt % Pt/MoO_2, and 20 wt % $Pt/Ti_{0.7}Mo_{0.3}O_2$ catalyst for comparison as shown in Figure S8 (Supporting Information). From this figure, it is clear that the Pt/undoped TiO_2 catalyst shows much lower ORR activity than either Pt/MoO_2 or $Pt/Ti_{0.7}Mo_{0.3}O_2$, which may be a result of the low electrical conductivity of TiO_2.[28] In contrast, the ORR catalytic activity of 20 wt % Pt/MoO_2 exhibited high catalytic activity, similar to 20 wt % $Ti_{0.7}Mo_{0.3}O_2$ catalyst. This enhancement probably contributed to the high electrical conductivity and specific catalytic reactivity of molybdenum oxide.[37] However, the MoO_2 support for the Pt catalyst showed a degradation of activity after the stability test was run for 1000 cycles (Figure S9, Supporting Information). This behavior implies that the Pt/MoO_2 catalyst is unstable and vulnerable to dissolution during the potential scan (0−1.1 V vs NHE) in ORR. The data derived from our study show that introduction of Mo into the TiO_2 lattice is a viable approach to making a highly active catalyst with good durability for application in ORR.

4. CONCLUSIONS

We have developed a robust non-carbon $Ti_{0.7}Mo_{0.3}O_2$ support that demonstrates very high activity and durability for ORR compared with commercial Pt/C (E-TEK) and PtCo/C (E-TEK) catalysts. Our results suggest this enhancement is a result of electronic structure changes of Pt upon its synergistic interaction with the $Ti_{0.7}Mo_{0.3}O_2$ support compared to carbon, which biases the reaction toward completion. Noticeably, the $Pt/Ti_{0.7}Mo_{0.3}O_2$ catalyst exhibits much higher stability than carbon-supported catalysts, which can be attributed to the large amount of surface Pt metal binding sites on the $Ti_{0.7}Mo_{0.3}O_2$ support. This facilitates the strong metal/support interactions (SMSI) between Pt particles and $Ti_{0.7}Mo_{0.3}O_2$ as well as enhancing the inherent structural and chemical stability and the corrosion resistance of $Ti_{0.7}Mo_{0.3}O_2$ in acidic and oxidative environments. The above findings undoubtedly show that the suggested approach for designing a robust non-carbon catalyst is effective and not only can be applied to PEMFCs but also can be extended to other fuel cells or areas, such as biosensor technology. The results of this work also indicate strategies suitable for incorporation of other dopants in TiO_2, as well as raising the possibility of using other oxides in alternative catalyst supports that opens a reliable path to the discovery advanced concept of designing new catalysts that can replace the traditional catalytic structure and motivate further research in the field.

■ ASSOCIATED CONTENT

Supporting Information. Complete ref 18, additional text describing calculation of the number of unfilled d-states (h_{Ts}), and nine figures showing EDX spectrum of $Ti_{0.7}Mo_{0.3}O_2$ support material, TEM of $Pt/Ti_{0.7}Mo_{0.3}O_2$, EDX spectrum and elemental mapping of $Pt/Ti_{0.7}Mo_{0.3}O_2$ catalyst, Mo K near-edge spectra of $Ti_{0.7}Mo_{0.3}O_2$, $Pt/Ti_{0.7}Mo_{0.3}O_2$, MoO_2, and MoO_3, comparison of ORR activities on mass activity of $Pt/Ti_{0.7}Mo_{0.3}O_2$ and commercial catalysts, polarization curves for ORR performance

on $Pt/Ti_{0.7}Mo_{0.3}O_2$ and commercial catalysts in O_2-saturated 0.1 M $HClO_4$ solution and on Pt/undoped-TiO_2, Pt/MoO_2, and $Pt/Ti_{0.7}Mo_{0.3}O_2$ catalysts in O_2-saturated 0.5 M H_2SO_4 solution, and polarization curves for Pt/MoO_2 before and after 500 and 1000 cycles. This material is available free of charge via the Internet at http://pubs.acs.org/.

AUTHOR INFORMATION

Corresponding Author

bjh@mail.ntust.edu.tw

Present Addresses

[§]National Taiwan University of Science and Technology, Taipei 106, Taiwan

ACKNOWLEDGMENT

We are grateful for support from the National Science Council (NSC), given under a special program for Nanoscience and Nanotechnology Research (Grants NSC-99-2120-M-011-001 and NSC 99-2811-M-011-005). We also thank the National Synchrotron Radiation Research Center (NSRRC) for providing facilities for the collection of X-ray absorption data.

REFERENCES

(1) Wang, C.; van der Vliet, D.; More, K. L.; Zaluzec, N. J.; Peng, S.; Sun, S.; Daimon, H.; Wang, G.; Greeley, J.; Pearson, J.; Paulikas, A. P.; Karapetrov, G.; Strmcnik, D.; Markovic, N. M.; Stamenkovic, V. R. *Nano Lett.* **2011**, *11*, 919.

(2) Gasteiger, H. A.; Kocha, S. S.; Sompalli, B.; Wagner, F. T. *Appl. Catal., B* **2005**, *56*, 9.

(3) Vielstich, W.; Lamm, A.; , Gasteiger, H. A. *Handbook of Fuel Cells: Fundamentals Technology and Applications*; Wiley: West Sussex, U.K., 2003.

(4) Ghosh, T.; Vukmirovic, M. B; DiSalvo, F. J.; Adzic, R. R. *J. Am. Chem. Soc.* **2010**, *132*, 906.

(5) Mazumder, V.; Chi, M.; More, K. L.; Sun, S. *J. Am. Chem. Soc.* **2010**, *132*, 7848.

(6) Zhang, J.; Yang, H.; Fang, J.; Zou, S. *Nano Lett.* **2010**, *10*, 638.

(7) Yang, H. *Angew. Chem., Int. Ed.* **2011**, *50*, 2674.

(8) Snyder1, J.; Fujita, T.; Chen, M. W.; Erlebacher, J. *Nat. Mater.* **2010**, *9*, 904.

(9) Mukerjee, S.; Srinivasan, S. *J. Electroanal. Chem.* **1993**, *357*, 201.

(10) Greeley, J.; Stephens, I. E. L; Bondarenko, A. S.; Johansson, T. P.; Hansen, H. A.; Jaramillo, T. F.; Rossmeisl, J.; Chorkendorff, I.; Nørskov, J. K. *Nat. Chem.* **2009**, *1*, 552.

(11) Srivastava, R.; Mani, P.; Hahn, N.; Strasser, P. *Angew. Chem., Int. Ed.* **2007**, *46*, 8988.

(12) Peter, S.; Shirlaine, K.; Toyli, A.; Jeff, G.; Karren, M.; Chengfei, Y.; Zengcai, L.; Sarp, K.; Dennis, N.; Hirohito, O.; Michael, F. T.; Anders, N. *Nat. Chem.* **2010**, *2*, 454.

(13) Nilekar, A. U.; Xu, Y.; Zhang, J.; Vukmirovic, M. B.; Sasaki, K.; Adzic, R. R.; Mavrikakis, M. *Top. Catal.* **2007**, *46*, 276.

(14) Loukrakpam, R.; Luo, J.; He, T.; Chen, Y.; Xu, Z.; Njoki, P. N.; Wanjala, B. N.; Fang, B.; Mott, D.; Yin, J.; Klar, J.; Powell, B.; Zhong, C.-J. *J. Phys. Chem. C* **2011**, *115*, 1682.

(15) Antolini, E.; Salgado, J. R. C.; Gonzalez, E. R. *J. Power Sources* **2006**, *160*, 957.

(16) Gasteiger, H. A.; Kocha, S. S.; Sompalli, B.; Wagner, F. T. *Appl. Catal., B* **2005**, *56*, 9.

(17) Jun, M.-S.; Zhang, Q.; Cao, A.; Su, D. S.; Zhang, Z.; Yoon, S.-H.; Miyawaki, J.; Mochida, I.; Kang, F. *Adv. Funct. Mater.* **2011**, *21*, 999.

(18) Borup, R.; et al. *Chem. Rev.* **2007**, *107*, 3904.

(19) Zhang, S.; Yuan, X.; Wang, H.; Mérida, W.; Zhu, H.; Shen, J.; Wu, S.; Zhang, J. *Int. J. Hydrogen Energy* **2009**, *34*, 388.

(20) Wang, Z.-B.; Zhao, C.-R.; Shi, P.-F.; Yang, Y.-S; Yu, Z.-B.; Wang, W.-K.; Yin, G.-P. *J. Phys. Chem. C* **2010**, *114*, 672.

(21) Fang, B.; Chaudhari, N. K.; Kim, M.-S.; Kim, J. H.; Yu, J.-S. *J. Am. Chem. Soc.* **2009**, *131*, 15330.

(22) Bagotsky, V. S. *Fuel Cells: Problems and Solutions*; Wiley: New York, 2009.

(23) Chung, Y.; Pak, C.; Park, G.-S.; Jeon, W. S.; Kim, J.-R.; Lee, Y.; Chang, H.; Seung, D. *J. Phys. Chem. C* **2008**, *112*, 313.

(24) Park, G. S.; Pak, C.; Chung, Y.-S.; Kim, J.-R.; Jeon, W. S.; Lee, Y.-H.; Kim, K.; Chang, H.; Seung, D. *J. Power Sources* **2008**, *176*, 48.

(25) Shao-Horn, Y.; Sheng, W. C.; Chen, S.; Ferreira, P. J.; Holby, E. F.; Morgan, D. *Top. Catal.* **2007**, *46*, 285.

(26) Antolini, E.; Gonzalez, E. R. *Solid State Ionics* **2009**, *180*, 746.

(27) Subban, C. V.; Zhou, Q.; Hu, A.; Moylan, T. E.; Wagner, F. T.; DiSalvo, F. J. *J. Am. Chem. Soc.* **2010**, *132*, 17531.

(28) Huang, S. Y.; Ganesan, P.; Park, S.; Popov, B. N. *J. Am. Chem. Soc.* **2009**, *131*, 13898.

(29) Jang, S. E.; Kim, H. *J. Am. Chem. Soc.* **2010**, *132*, 14700.

(30) Ko, Y. J.; Oh, H. S.; Kim, H. *J. Power Sources* **2010**, *195*, 2623.

(31) Shao, Y.; Yin, G.; Gao, Y.; Shi, P. *J. Electochem. Soc.* **2006**, *153*, A1093.

(32) Oh, H. S.; Lim, K. H.; Roh, B.; Hwang, I.; Kim, H. *Elecrochim. Acta.* **2009**, *54*, 6515.

(33) Kou, R.; Shao, Y.; Wang, D.; Engelhard, M. H.; Hwak, J. H.; Wang, J.; Viswanathan, V. V.; Wang, C.; Lin, Y.; Wang, Y.; Aksay, I. A.; Liu, J. *Electrochem. Commun.* **2009**, *5*, 954.

(34) Wang, D.; Subban, C. V.; Wang, H.; Rus, E.; DiSalvo, F. J.; Abruña, H. D. *J. Am. Chem. Soc.* **2010**, *132*, 10218.

(35) Pourbaix, M. *Atlas of Electrochemical Equilibria in Aqueous Solutions*; NACE International: Houston, TX, 1974.

(36) Aryanpour, M.; Hoffmann, R.; DiSalvo, F. J. *Chem. Mater.* **2009**, *21*, 1627.

(37) Zhang, H.; Wang, Y.; Fachini, E. R.; Cabrera, C. R. *Electrochem. Solid-State Lett.* **1999**, *2*, 437.

(38) Yoshimura, M.; Byrappa, K. *J. Mater. Sci.* **2008**, *43*, 2085.

(39) Hwang, B. J.; Kumar, S. M. S.; Chen, C. H.; Chang, R. W.; Liu, D. G.; Lee, J. F. *J. Phys. Chem. C* **2008**, *112*, 2370.

(40) Lai, F. J.; Sarma, L. S.; Chou, H. L; Liu, D. G.; Hsieh, C. A.; Lee, J. F.; Hwang, B. J. *J. Phys. Chem. C* **2009**, *113*, 12674.

(41) Carmo, M.; dos Santos, A. R.; Poco, J. G. R.; Linardi, M. *J. Power Sources* **2007**, *173*, 860.

(42) Ressler, T.; Timpe, O.; Neisius, T.; Find, J.; Mestl, G.; Dieterle, M.; Schlogl, R. *J. Catal.* **2000**, *191*, 75.

(43) Kutzler, F. W.; Natoli, C. R.; Misemer, D. K.; Doniach, S.; Hodgson, K. O. *J. Chem. Phys.* **1980**, *73*, 3274.

(44) Ebbinghaus, S.; Hu, Z.; Reller, A. *J. Solid State Chem.* **2001**, *156*, 194.

(45) Ressler, T.; Jentoft, R. E.; Wienold, J.; Günter, M. M.; Timpe, O. *J. Phys. Chem. B* **2000**, *104*, 6360.

(46) Hwang, B.-J.; Sarma, L. S.; Chen, J.-M.; Chen, C.-H.; Shih, S.-C.; Wang, G.-R.; Liu, D.-G.; Lee, J.-F.; Tang, M.-T. *J. Am. Chem. Soc.* **2005**, *127*, 11140.

(47) Wang, D.-Y.; Chen, C.-H.; Yen, H.-C.; Lin, Y.-L.; Huang, P.-Y.; Hwang, B.-J.; Chen, C.-C. *J. Am. Chem. Soc.* **2007**, *129*, 1538.

(48) Hwang, B. J.; Murugesan, S.; Kumar, S.; Chen, C.-H.; Monalisa; Cheng, M.-Y.; Liu, D.-G.; Lee, J.-F. *J. Phys. Chem. C* **2007**, *111*, 15267.

(49) Tauster, S. J.; Fung, S. C.; Garten, R. L. *J. Am. Chem. Soc.* **1978**, *100*, 170.

(50) Shih, C. C.; Chang, J. R. *J. Catal.* **2006**, *240*, 137.

(51) Krstajic, N. V.; Vracar, L. M.; Radmilovic, V. R.; Neophytides, S. G.; Labou, M.; Jaksic, J. M.; Tunold, R.; Falaras, P.; Jaksic, M. M. *Surf. Sci.* **2007**, *601*, 1949.

(52) Henderson, G. S.; Liu, X.; Fleet, M. E. *Phys. Chem. Mineral.* **2002**, *29*, 32.

(53) Zhang, S.; Ogale, S. B.; Yu, W.; Gao, X.; Liu, T.; Ghosh, S.; Das, G. P.; Wee, A. T. S.; Greene, R. L.; Venkatesan, T. *Adv. Mater.* **2009**, *21*, 2282.

(54) Schmidt, T. J.; Gasteiger, H. A.; Stab, G. D.; Urban, P. M.; Kolb, D. M.; Beh, R. J. *J. Electrochem. Soc.* **1998**, *145*, 2354.
(55) Brezesinski, T.; Wang, J.; Tolbert, S. H.; Dunn, B. *Nat. Mater.* **2010**, *9*, 146.
(56) Shi, Y.; Guo, B.; Corr, S. A.; Shi, Q.; Hu, Y.-S.; Heier, K. R.; Chen, L.; Seshadri, R.; Stucky, G. D. *Nano Lett.* **2009**, *9*, 4215.
(57) Liu, X.-X.; Bian, L.-J.; Zhang, L.; Zhang, L.-J. *J. Solid-State Electrochem.* **2007**, *11*, 1279.
(58) Stamenkovic, V. R.; Mun, B. S.; Arenz, M.; Mayrhofer, K. J. J.; Lucas, C. A.; Wang, G.; Ross, P. N.; Markovic, N. M. *Nat. Mater.* **2007**, *6*, 241.
(59) Kim, J.; Lee, Y.; Sun, S. *J. Am. Chem. Soc.* **2010**, *132*, 4996.
(60) Stamenkovic, V. R.; Fowler, B.; Mun, B. S.; Wang, G.; Ross, P. N.; Lucas, C. A.; Marković, N. M. *Science* **2007**, *315*, 493.